Wake induced by an undulating elephant seal whisker

Joseph Bunjevac, Jodi Turk, Aidan Rinehart & Wei Zhang

Journal of Visualization

ISSN 1343-8875

J Vis
DOI 10.1007/s12650-018-0484-4

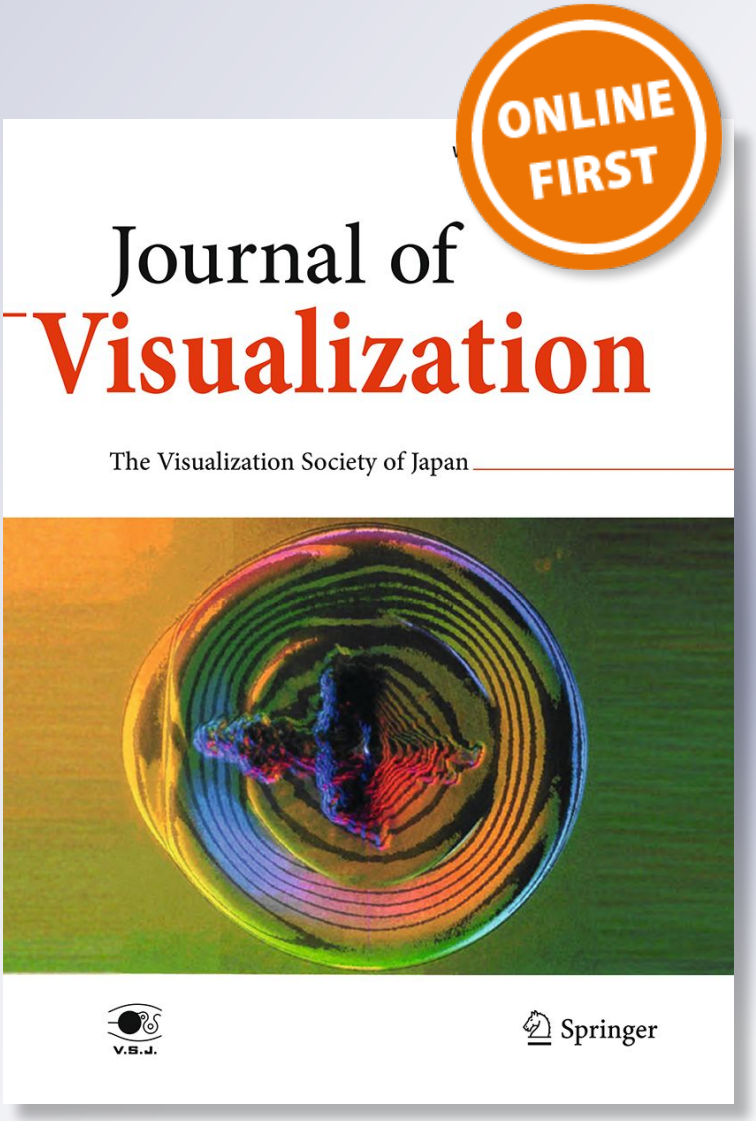

Springer

J Vis
https://doi.org/10.1007/s12650-018-0484-4

REGULAR PAPER

Joseph Bunjevac · Jodi Turk · Aidan Rinehart · Wei Zhang

Wake induced by an undulating elephant seal whisker

Received: 2 November 2017 / Revised: 23 January 2018 / Accepted: 28 January 2018

Abstract Certain species of seals are able to faithfully detect minute disturbances in ambient water solely using their whiskers, which is attributed to the whiskers' undulating three-dimensional (3D) morphology. While previous studies have examined effects of key morphology parameters on the wake using scaled-up whisker models, it is unclear how the wake behaves when induced by a real undulating seal whisker. Real seal whiskers usually have a diameter of about one millimeter and present variation in size and bending curvature along the length, which are not being considered in designing scaled-up whisker-like models. In addition, how the whisker orientation affects the induced wake and vortex shedding needs to be clarified. This work examines the wake flow characteristics generated by a real elephant seal whisker (of undulating morphology) and a California sea lion whisker (of smooth morphology) in laboratory water channels at Reynolds numbers of 110 and 390, using snapshot particle image velocimetry (PIV) and time-resolved PIV methods. Results indicate that the reversed flow region is remarkably reduced and turbulence intensities are greatly suppressed behind the undulating whisker compared to that of the smooth whisker, when the major axis of the whisker cross-section is parallel with the incoming flow (i.e., the angle of attack or AOA is 0°). While the vortex shedding frequency is reduced for both the undulating and smooth whiskers, the power spectral density is substantially increased at an AOA = 90° in comparison to AOA = 0°. Regardless of the AOA, the power spectral density is approximately 40% lower in the wake of the undulating whisker than that of the smooth whisker, indicating the favorable hydrodynamic feature of the undulating whisker. The extraordinary hydrodynamic traits of undulating seal whiskers is promising for renovating aero-propulsion flow components and designing high-sensitivity underwater flow sensors.

Keywords Seal whisker · Vortex shedding · Vortex-induced vibration (VIV) · Biomimicry · Whisker-inspired applications

J. Bunjevac · J. Turk · A. Rinehart · W. Zhang (✉)
Mechanical Engineering Department, Cleveland State University, Cleveland 44115, OH, USA
E-mail: w.zhang13@csuohio.edu
Tel.: +216-687-2595

J. Bunjevac
E-mail: j.bunjevac@vikes.csuohio.edu

J. Turk
E-mail: j.c.turk@vikes.csuohio.edu

A. Rinehart
E-mail: aidan.rinehart@gmail.com

Published online: 12 March 2018

1 Introduction

Seals with whiskers (vibrissae) of undulating morphology, which are the majority of true seals (Phocids), can trace even minute disturbance caused by prey fish in the ambient flow using only sensory input from their whiskers (Dehnhardt and Kaminski 1995; James and Dykes 1978; Renouf and Gaborko 1982). The superior sensing capability of harbor seal whiskers is attributed to the suppression or augmentation of vortex induced vibration (VIV), generated by bluff-bodies in air or water flow paths. In particular, the capability of seal whiskers to suppress the VIV and reduce drag is of great interest. Mimicking the beaded whisker morphology can be adopted as a passive flow control strategy in broad spectra of engineering applications, including structures in consistent flow paths such as wind turbine towers, light posts, high-rise buildings, sensor mounting supports on aircraft frames, and offshore oil drilling rigs. Research efforts have been made to design whisker-like high-sensitivity flow sensors (Beem 2015) and to modify the geometry of gas-turbine blades for enhanced aerodynamic performance in off-design conditions (Shyam et al. 2015). Applications of biomimetic flow control in engineered propeller have also been considered (Fish et al. 2008).

The morphology of a typical harbor seal whisker can be seen as an ellipsoidal cross-section with a repeating sequence of peaks and troughs along its length (Fish et al. 2008; Ginter et al. 2010, 2012). Interestingly, the elliptical cross-section is inclined with respect to the whisker axis and this inclination varies from whisker bottom to tip. A framework of seven parameters is used to describe the undulating three-dimensional morphology, Fig. 1, has been introduced and used widely in related works (Hanke et al. 2010). The peak is characterized by a major axis radius, a, a minor axis radius, b, and an angle of incidence, α. Similarly, the trough is described by the major axis radius, k, the minor axis radius, l, and the angle of incidence, β. Also, the half wavelength, M, is the distance between a peak and a trough. Using computer-tomography (CT) scanning data of the morphology of beaded seal whiskers (harbor seal and elephant seal), we confirmed that the length parameters are generally consistent across various studies, but found that the angle of incidence(α and β) of elliptical cross-sections varies in a wide range with a majority falling between -5° and 5°. Statistical analysis of angles of incidence at both peaks and troughs resulted in a quasi-Gaussian distribution, but no clear preference of orientation was identified (Rinehart et al. 2017).

While experiments have been conducted with seals to understand how their whiskers function in a controlled environment, there are only limited studies that directly measure the wake flow generated by real whisker samples. Hanke et al. (2010) and Witte et al. (2012) reported experimental results of flow in a very small region adjacent to a real whisker using a micro-particle imaging velocimetry (μPIV). The work relied on detailed numerical simulations to demonstrate the wake hydrodynamics, such as drag and lift coefficients and vortex shedding. Murphy (2013) measured a cantilever-mounted whisker's shaft vibration by laser vibrometry; no wake flow information was reported. While it is a bit surprising that no distinct difference in vibration frequency and amplitude is found for the undulating and smooth whiskers, the work revealed the noticeable effects of the angle of attack (AOA) on whisker vibration frequency and amplitude. Their recent follow-up in-situ experiment revealed a broader range of the whisker vibration, frequencies of 100–300 Hz, of living seals while swimming. The vibrations of seal whiskers may provide information about hydrodynamic events and enable sophisticated wake-tracking abilities of these animals (Murphy et al. 2017).

Limited studies about the wake flow around a real whisker have been conducted. Challenges may arise owing to variations related to biology species and the small physical size, approximately 0.5–1 mm, of the nominal diameter of the whisker. Research also showed that the bio-mechanics characteristics of seal whiskers may change after being removed from living seals (Hans et al. 2014). Instead, by employing scaled-up whisker-like rigid models, extensive experimental research has been done to examine the effects of key whisker morphology parameters (Wang and Liu 2016). This line of research is well aligned with the passive flow control using modified surface geometry of cylindrical cylinders or wavy cylinders (Lin et al. 2016; Zhang et al. 2005). The ability of modified geometries to suppress vortex-induced vibrations and reduce the drag forces acting upon them has been the central subject of various experimental and numerical studies (Morrison et al. 2016; Kim and Yoon 2017; Lin et al. 2016; Wang and Liu 2016). The flow properties of these modified cylinder geometries, along with the resulting forces, are generally comparable to those observed for the undulating seal whiskers (Morrison et al. 2016).

Measurements of the vibration forces acting on the whisker in a uniform flow by Miersch et al. (2011) show that self-induced vibration by a vortex street is about ten times lower for a harbor seal whisker. Recognizing that current flows can vary in direction with respect to the whisker, the AOA could be a critical factor when adopting the whisker-like morphology parameters. Unfortunately the effect of the AOA has not been extensively studied for the wake flow induced by a whisker. Miersch et al. (2011) tested the whisker

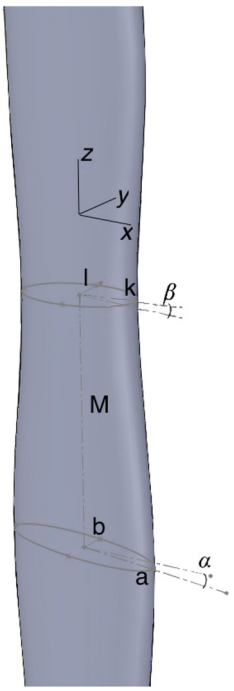

Fig. 1 Definition of the seven parameters of the whisker morphology, introduced by Hanke et al. (2010). The peak defined by the major radii, a, and minor axis radii, b, and angle of incidence, α. The distance between peak and trough is M. The trough defined by the major radii, k, and minor axis radii, l, and angle of incidence, β

vibration at three typical angles of attack (AOA = 0°, 45° and 90°) without providing wake flow information. Kim and Yoon (2017) applied numerical simulation to analyze instantaneous 3-D vortex structures, drag and lift coefficients, as well as the vortex shedding at the AOA range of 0°–90° for a Reynolds number of 500. To our best knowledge, no experimental studies have been conducted to understand the interaction of the vortex shedding and the coupled vibration.

This study aims to characterize the wake flow and the vortex shedding induced by a real undulating seal whisker in well-controlled water channels. Two different real seal whiskers are used: one is the elephant seal whisker with typical undulating morphology and the other is a similar-size California sea lion whisker of smooth morphology. We first described the PIV measurements of the wake flow induced by real undulating and smooth whiskers. In particular, the challenges of locating the light-sheet at desired planes and handling the unique bending curvature of the whisker are discussed (Sect. 2). Then we showed flow statistics of the wake induced by the undulating and the smooth whiskers in two orthogonal planes at an AOA = 0° (Sect. 3). We further evaluated the strength and frequency of the vortex shedding behavior using the high-speed PIV data at AOA = 0° and 90°, which revealed the significant effect that the flow direction has on the vortex shedding (Sect. 3). The contribution is primarily twofold: (1) This work provided a detailed characterization of the wake flow and vortex shedding induced by single isolated real undulating and smooth whiskers, which is different from related studies which used scaled-up whisker-like models that commonly do not allow a full capture of the whisker morphology. The observed wake flow statistics and vortex shedding are expected to well reflect what occurs in nature. (2) The effects of the AOA on vortex shedding are illustrated between the undulating and smooth whiskers. The finding reveals a distinctly lower strength of the vortex shedding by the undulating whisker compared to the smooth whisker, consistent with statistics of wake flow.

2 Experimental setup and measurement methods

2.1 Laboratory water channels

Two water channels of similar flow quality are employed in this study, Fig. 2. The water channel at Cleveland State University (CSU) has a test section of 0.14 m (W)× 0.20 m (H) × 0.61 m (L). The flow is

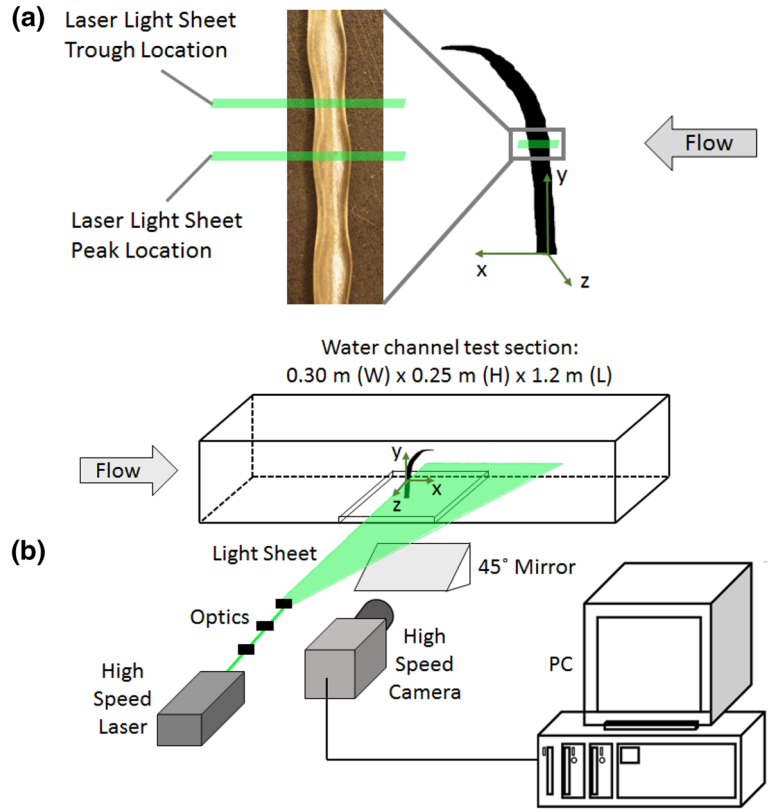

Fig. 2 **a** Measurement planes at the peak and trough of an undulating whisker. **b** Schematics of the high-speed PIV measurement setup. The Cartesian coordinate is originated at the base of the single whisker. The x, y and z coordinates correspond to streamwise, vertical and spanwise directions and the velocities are u, v and w, respectively

conditioned by six one-inch thick honeycombs spaced one-inch apart with 6.35 mm openings, 0.2 m upstream from the test section. Another water channel, at the Biofluid and Biomimic Research Center (BBRC) of Pohang University of Science and Technology (POSTECH) in Pohang, South Korea, has a test section of 0.30 m (W) × 0.25 m (H) × 1.2 m (L). The flow properties in the test sections of both water channels were characterized using PIV data prior to studying the whisker wake flow. In the CSU water channel, the free-stream velocity, U_0, was constant at 0.12 m/s, yielding the Reynolds number of about 110 (based on U_0 and the whiskers hydraulic diameter D_h defined in Eq. 1). In the POSTECH water channel the free-stream velocity was set at a U_0 of 0.49 m/s, yielding the Reynolds number of about 390. Depending on the seals swimming speed and the whiskers hydraulic diameter, the Reynolds number is usually in the order of 10^2 to 10^3 (Wang and Liu 2016). As the seal engages active hunting, its swimming speed reaches the order of 1,m/s (James and Dykes 1978). The present two Reynolds numbers are determined based on the capacity of flow facilities but still within the reasonable seals' swimming speed range (0.15–0.5 m/s used in Miersch et al. 2011; Witte et al. 2012 and Murphy et al. 2017).

It is also noted that, both water channels generate a uniform flow in the test section, where the real whisker is mounted for testing. The boundary-layer thickness on the smooth bottom and side walls is estimated to be 1–1.5 cm (less than 5% of the channel depth) at the half length downstream of the inlet, for a fully-developed boundary layer. The streamwise turbulence intensity in both water channels is at a similar level of 3–5%.

2.2 Real seal whiskers

The whisker samples are provided by the Marine Mammal Center, and previously used by Rinehart et al. (2017). The key parameters of an elephant seal whisker (of undulating morphology) and a California sea lion whisker (of smooth morphology) are listed in Table 1. It is noted that the angle of incidence α and β, of

elliptical cross-sections along the whisker length are not measured for the specific whiskers. However, they are assumed to fall into the range of -15° to 15° with a higher probability of being between -5° and 5° (Rinehart et al. 2017).

Given the variation of the morphology parameters along the whisker length D_h is used as the characteristic length scale. The hydraulic diameter is calculated by:

$$D_h = \frac{4 \cdot A}{P}, \tag{1}$$

where the area, A, and the circumference, P (via the Euler approximation) of an elliptical cross-section are as follows:

$$A = a \cdot b \cdot \pi, \tag{2}$$

$$P = 2 \cdot \pi \sqrt{\frac{a^2}{2} + \frac{b^2}{2}}. \tag{3}$$

2.3 Particle image velocimetry (PIV) measurements

Wake behind the real whiskers is measured by a two-dimensional two-component (2D2C) snap-shot PIV and a high-speed PIV system (see Fig. 2b). The former allows us to acquire converged turbulence statistics and the latter enables us to capture vortex shedding behavior induced by a seal whisker with sufficient temporal resolution.

The 2D2C snap-shot PIV system (LaVision GmbH) was used to measure random instantaneous velocity fields and evaluate the turbulence statistics. A laser light sheet was formed from a laser beam of an Evergreen dual-pulsed ND:Yag laser at 15 Hz and carefully aligned to the desired area of interest. The water was seeded with hollow glass spheres of 10 μm in diameter. The particle images were captured with a Pro-Imager SX 5MP CCD camera (of 2456 pixels × 2058 pixels) fitted with a Nikon AF Micro-Nikkor 60 mm lens. A total of 1200 image pairs were captured in each measurement plane for both whiskers. Calibration of the 2D2C PIV measurements was conducted by taking multiple images of a scale in the center of the field of view (FOV). The FOV is 35.38 mm by 12.98 mm in the horizontal planes and 79.85 mm by 66.91 mm in the vertical plane in the CSU water channel. The conversion factor of 69.41 pixels/mm (for the horizonal planes) and 30.76 pixels/mm (for the vertical plane) is used, respectively, to transform the data from image plane to the physical coordinates. The FOV covers 25–30 D_h downstream of the whisker in the horizontal planes and 60–70 D_h in the vertical central plane.

Properly aligning the light sheet with a real whisker sample is critical to get data at the desired measurement planes and interpret the results faithfully. Due to the real whiskers having a natural bending curvature, challenges emerge when aligning the laser light sheet to the whisker in the vertical central plane. The whisker was first attached to a 1.58 mm diameter rigid rod and then mounted on a thin plate at the bottom of the water channel. The coordination of the optics tube, laser mounting mechanism, and the modeling clay allowed the light sheet to cover the majority of the mid-section of the whisker in the vertical plane. For the horizontal planes, the light sheet was aligned with a peak or trough or selected location. Alignment was monitored using a secondary camera with a telephoto lens to ensure proper placement of a light sheet at each peak and trough location.

Instantaneous vector fields from the snap-shot PIV tests were obtained with a window-based cross-correlation algorithm (DaVis 8.3, LaVision GmbH). A two-pass procedure was employed: initial interrogation window of 32 by 32 pixels followed by a reduced window of 16 by 16 pixels with 50% overlap in each pass. Convergence history of the mean streamwise velocity and the streamwise turbulence intensity at selected location of wake flow is examined with samples of 200, 300, 400, 600, 800, 1000 and 1200. The mean streamwise velocity reaches convergence at 400 instantaneous velocity fields, while the streamwise

Table 1 Morphology parameters of the elephant seal whisker (ES) and the Californian sea lion whisker (CSL)

Parameters	$2a$ mm	$2b$ mm	$2k$ mm	$2l$ mm	D_h mm	$D_{h,\text{peak}}$ mm	$D_{h,\text{trough}}$ mm	a / b	k / l
ES	0.978	0.521	0.826	0.495	–	0.650	0.601	1.88	1.67
CSL	0.991	0.686	–	–	0.797	–	–	1.44	–
ES (mean)	1.233	0.583	1.099	0.642	0.890	–	–	2.12	1.71

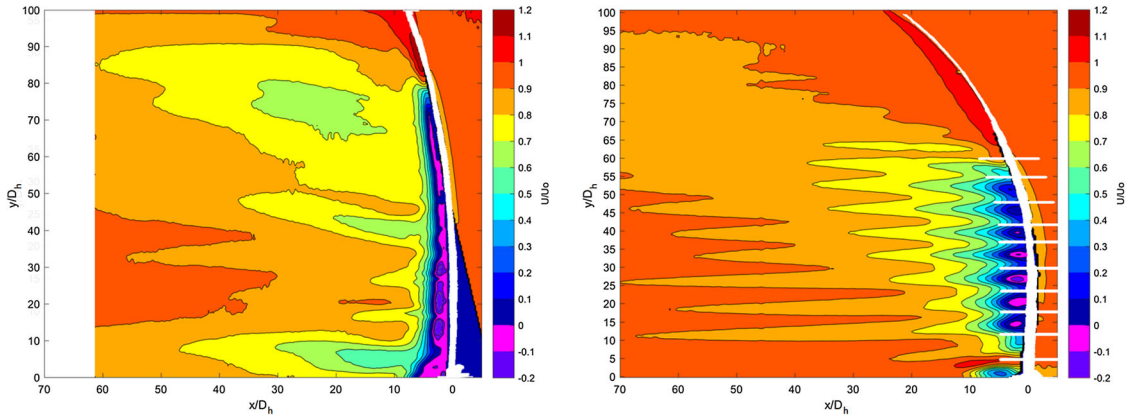

Fig. 3 Mean streamwise velocity (U/U_0) of the wake induced by the California sea lion whisker (Smooth, left) and the elephant seal whisker (Undulating, right) at Re = 110. White horizontal lines mark the peak locations of the undulating whisker. Flow is from right to left

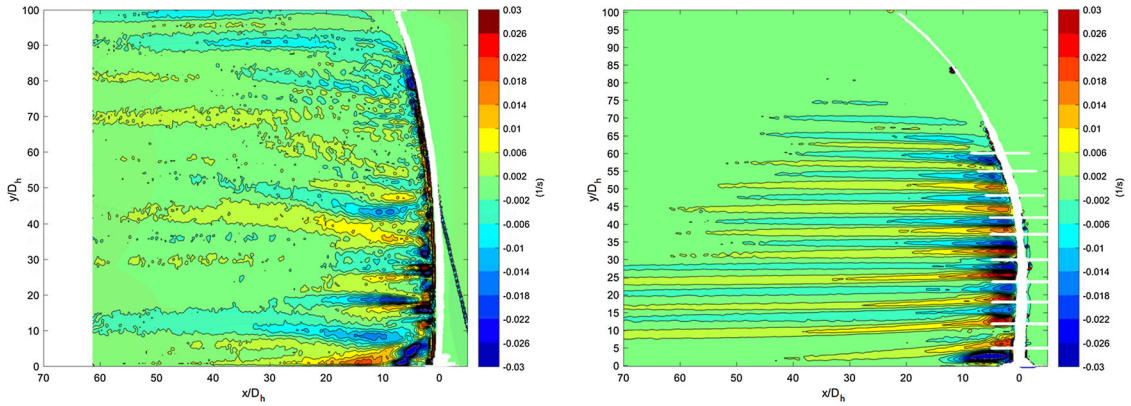

Fig. 4 The spanwise vorticity (ω_z, 1/s) of the wake induced by the California sea lion whisker (Smooth, left) and the elephant seal whisker (Undulating, right) in the vertical central plane at Re = 110. Flow is from right to left

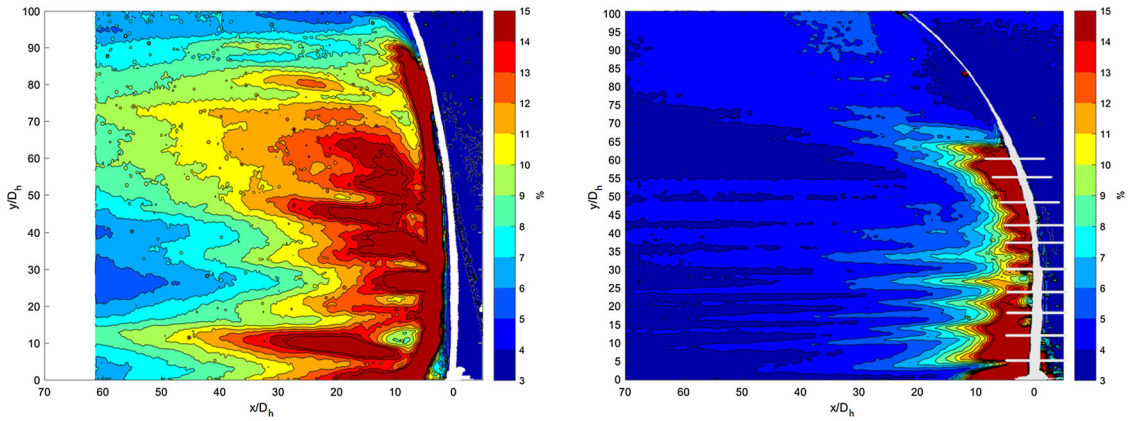

Fig. 5 Streamwise turbulence intensity I_u in the wake induced by the sea lion whisker (smooth, left) and the California elephant seal whisker (undulating, right) in the vertical central plane at Re = 110. Flow is from right to left

turbulence intensity needs 1000 samples for convergence. All 1200 instantaneous velocity fields were ensemble-averaged to ensure convergence of computing the mean velocity and turbulence statistics of the wake flow.

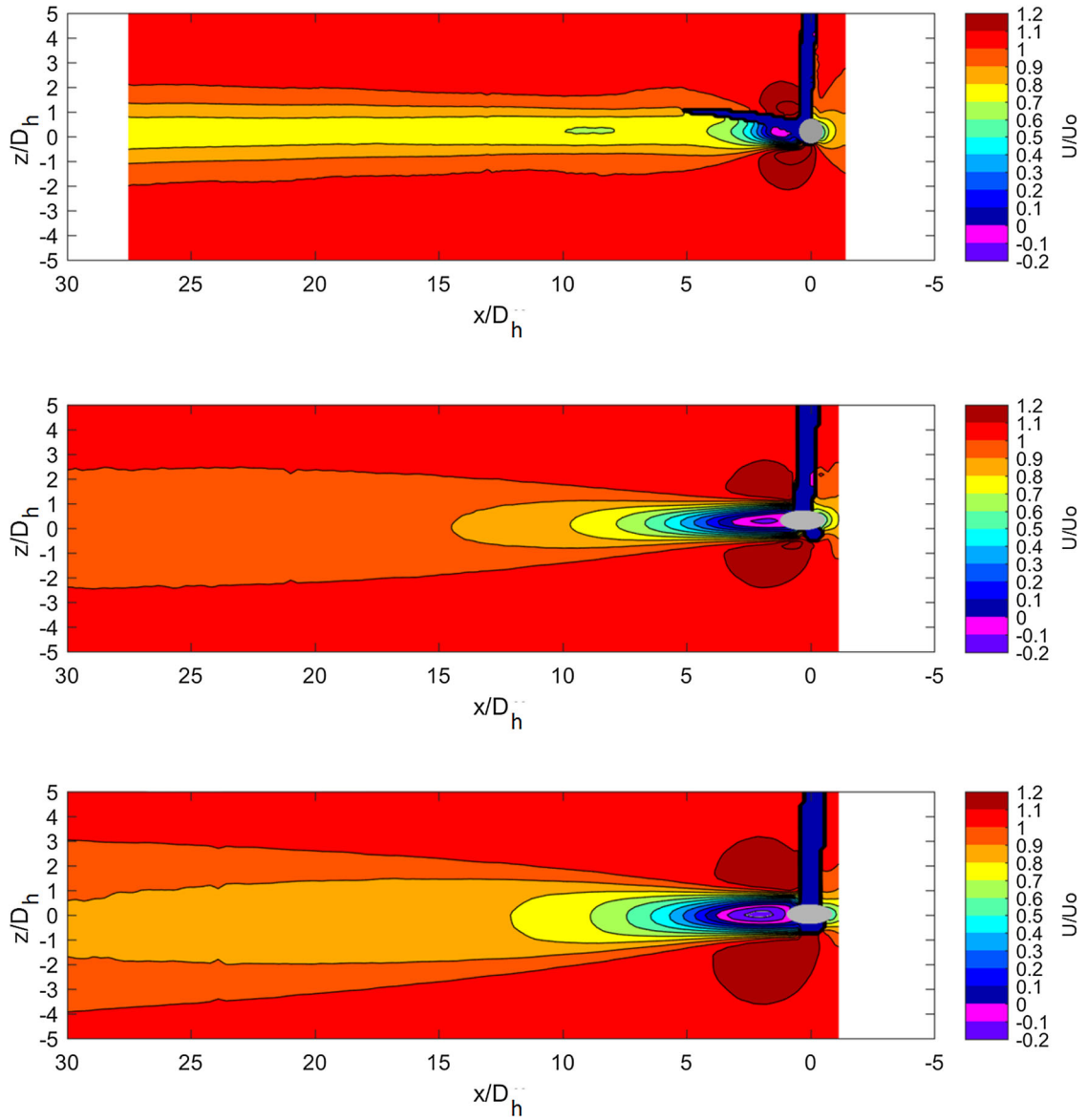

Fig. 6 Mean streamwise velocity (U/U_0) of the wake induced by the smooth California sea lion whisker (top), the peak (middle) and the trough of the undulating elephant seal whisker (bottom) in the horizontal planes at Re = 110. Flow is from right to left

The high-speed PIV system at POSTECH was used to analyze the vortex shedding behavior of the wake by both whiskers. The experimental set-up is very similar to that of the snap-shot PIV, as shown in Fig. 2. The water channel is seeded with silver hollow spheres that have a mean diameter of 44 μm. The particle images were taken at peak and trough locations only in the horizontal plane at a rate of 5000 frames per second (fps), with a Fastcam SA1.1 Photron High Speed Camera and a Nikon ED AF Micro Nikkor 200 mm 1:4D Lens (fitted with a Nikon L37c 62 mm filter). The FOV of the particle images taken in the POSTECH water tunnel is 23.33 mm by 23.33 mm with the camera resolution of 1024 pixels by 1024 pixels. The conversion factor of 43.89 pixels/mm is used to transform the data from image plane to the physical plane. A total of 8000 images were captured for each measurement plane and analyzed using the window-based correlation method. The Cartesian coordinate system was the same as the 2D2C snap-shot PIV experiments. The measurement uncertainty is also similar to that of the snap-shot PIV tests. It is noted that no ensemble-averaging is performed for flow statistics computation, instead, behavior of the vortex shedding is the focus of the time-resolved PIV results.

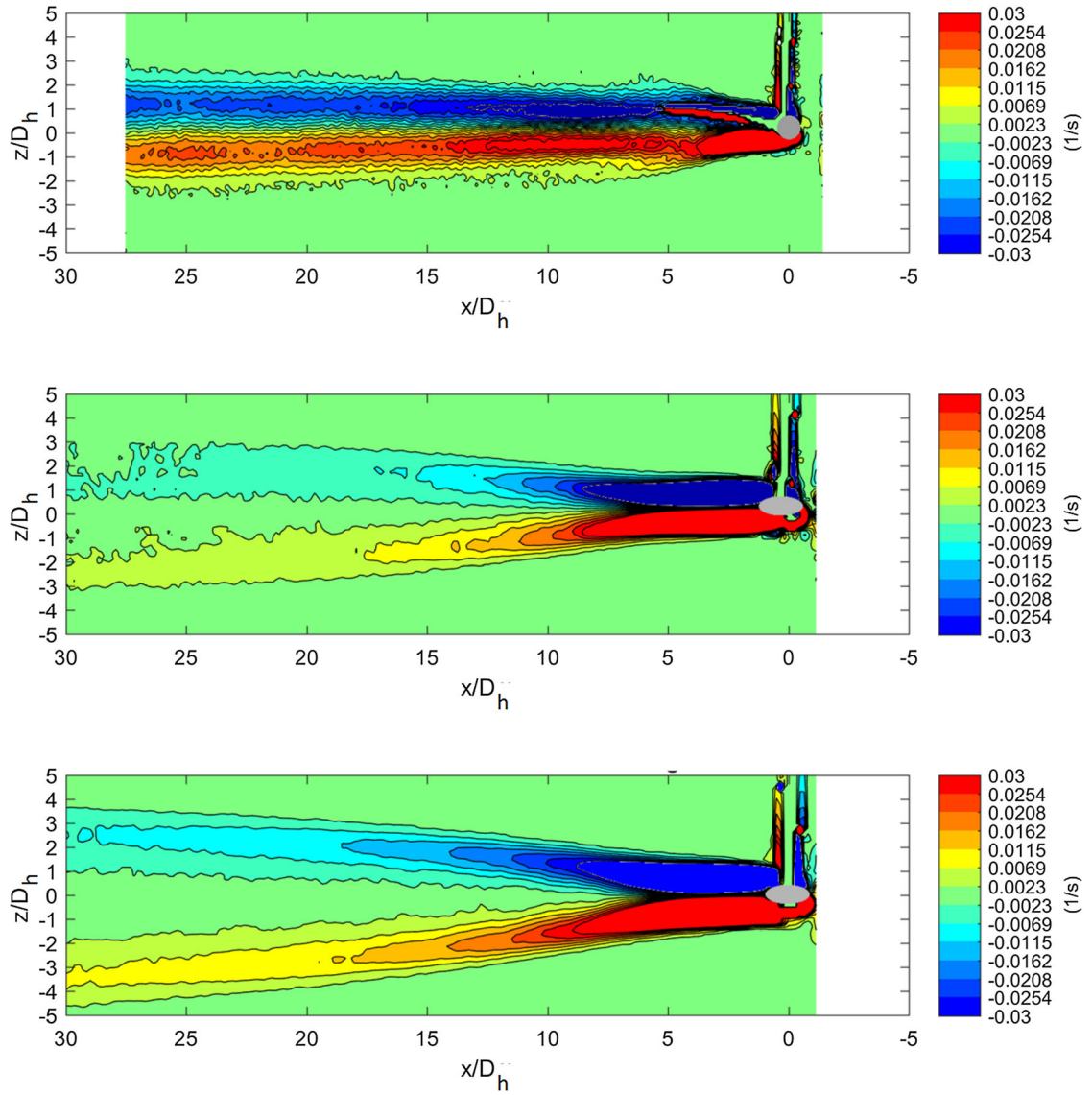

Fig. 7 Vertical vorticity (ω_y, 1/s) of the wake induced by the smooth California sea lion whisker (top), the peak (middle) and the trough of the undulating elephant seal whisker (bottom) in the horizontal planes at Re = 110. Flow is from right to left

2.4 PIV measurement uncertainty

The total PIV measurement uncertainty is contributed collectively by various possible error sources, including the experimental setup, data acquisition, particle image quality, and data processing/post-processing (Adrian and Westerweel 2011; Raffel et al. 2007). Measurement uncertainty is also dependent on the specific flow features under investigation. Significant bias errors can be minimized by following PIV experimental guidelines and the random errors for a standard planar PIV are primarily determined by how accurately the cross-correlation peaks can be measured (Raffel et al. 2007). In both snap-shot PIV and high-speed PIV measurements, the correlation peaks were estimated to be about 0.1 pixel accuracy with the multi-iteration cross-correlation algorithm (Keane and Adrian 1993). The particle displacements were nominally 7–8 pixels in the far wake and the free stream but reduced to be about 2–3 pixels in the near wake region. Hence, the random error in the 2C PIV measurements is roughly 1.4 and 5% of full scale. Ensemble-averaging 1200 instantaneous velocity fields will result in the mean flow statistics in the near and far wakes below 1% of the full scale (by dividing it with $\sqrt{1200}$, Tavoularis 2005). The other option under

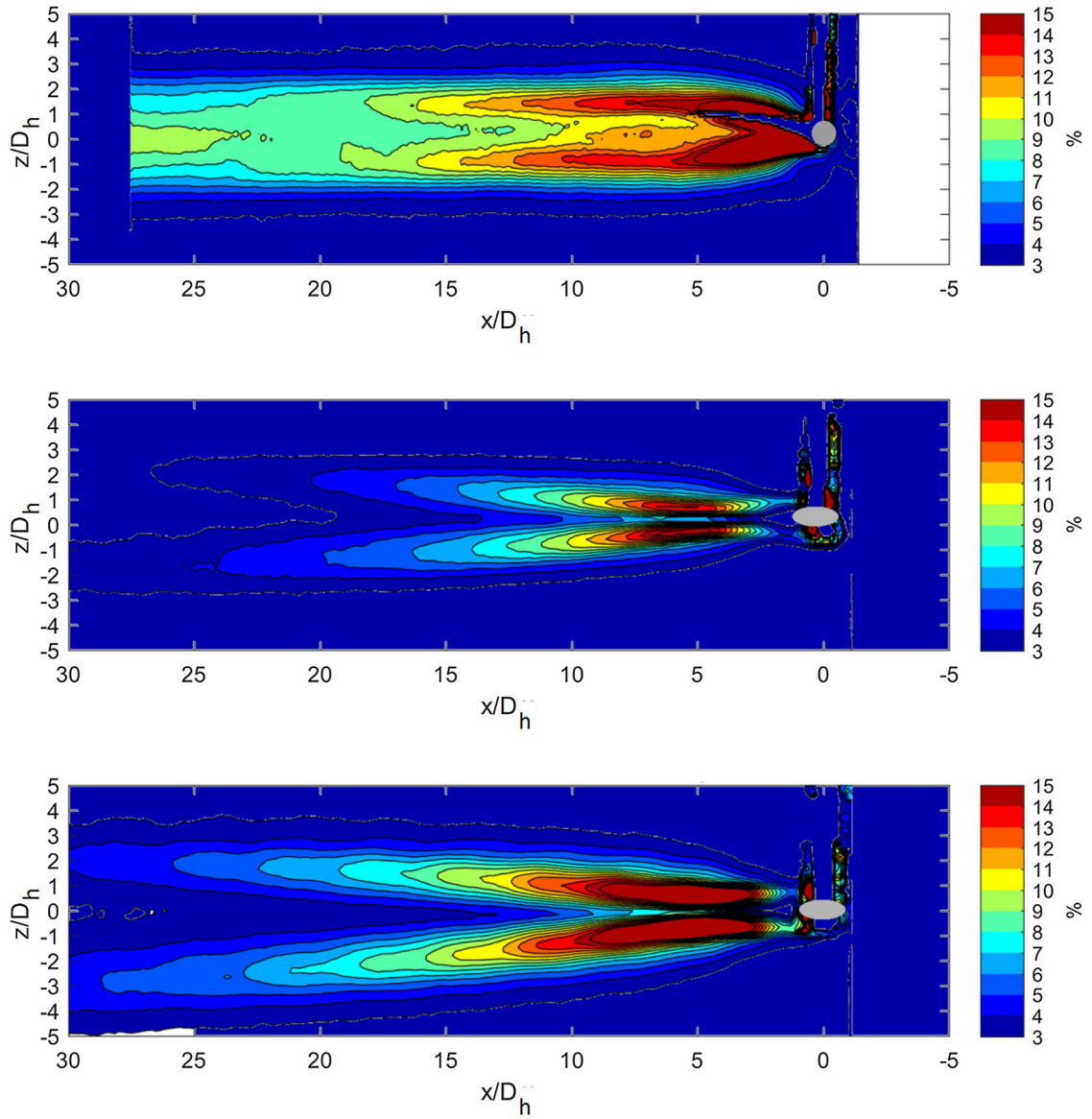

Fig. 8 Streamwise Turbulence Intensity I_u of the wake induced by the smooth California sea lion whisker (top), the peak (middle) and the trough of the undulating elephant seal whisker (bottom) in the horizontal planes at Re = 110. Flow is from right to left

consideration is to use the correlation statistics method to obtain the map of the random error by image matching (Wieneke 2015).

Another aspect of measurement uncertainty is the interaction of whisker vibration and the induced wake. Since the single whisker sample is mounted as a cantilever, it is subjected to VIV. Subsequently, the wake structure and vortex shedding is affected by the whisker vibration. To evaluate the effects of whisker vibration on flow statistics, several cases in the high-speed PIV tests are utilized to identify displacement of profiles of the whisker cross-section in horizontal planes (Re = 390). Results show that the whisker displacement in the streamwise direction is much less than that in the spanwise direction, thus only the displacement perpendicular to the inflow is considered. The smooth whisker displacement is $0.043\,D_h$ at an AOA = 0° and increased to $0.86\,D_h$ at an AOA = 90°. For the peak location of the undulating whisker, the displacement is $0.7\,D_h$ at an AOA = 90°. The magnitude of the whisker vibration agrees well with the strength of the vortex shedding (see Sect. 3.3). We conclude that the whisker vibration will have an influence on the flow statistics within $1D_h$ around the whisker at an AOA = 90° while this effect can be safely neglected at an AOA = 0°.

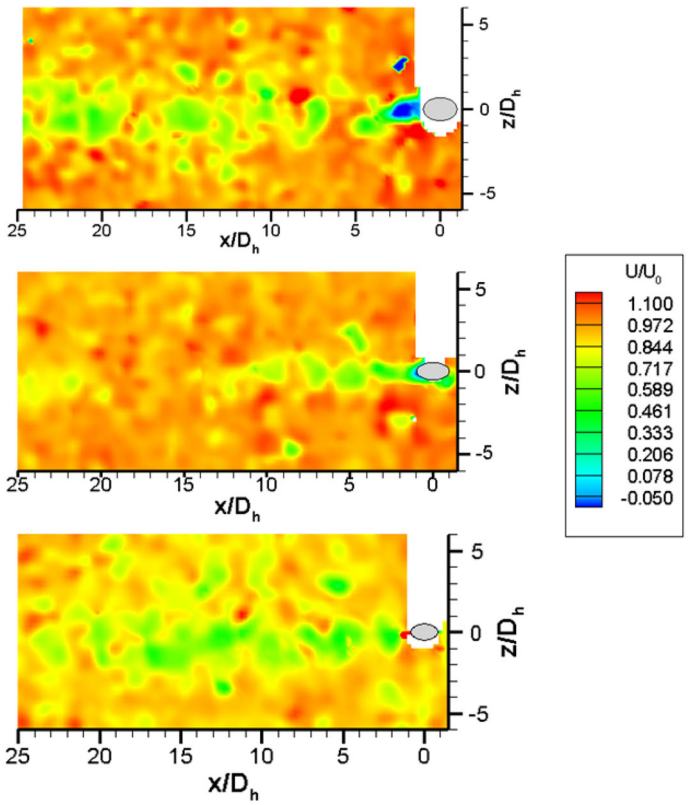

Fig. 9 Instantaneous streamwise velocity U/U_0 in the horizontal planes at Re = 390 and AOA = 0°. The smooth California sea lion whisker (top), the peak location (middle), and the trough location (bottom) of an undulating elephant seal whisker. Flow is from right to left

3 Results and discussion

3.1 Flow statistics of the wake: vertical central plane

The vertical central plane is a representative plane to observe the overall structure of the wake induced by a whisker. Note that the measurement plane is in the mid-section of the whisker covering the range of $y/D_h = 10{-}60$ and the data is only shown at an AOA = 0°. Both smooth and undulating whiskers are mounted in a consistent way such that the bending curvature is away from the inflow. The reversed flow zone immediately behind the smooth whisker varies in an irregular manner, which is speculated to be associated with the cross-section size change from bottom to tip. Otherwise, a uniform reversed flow region along the length is expected in the wake similar to that in Zhang et al. (2005). The wake of the smooth whisker recovers as it moves downstream, displaying strong heterogeneous distribution of the streamwise velocity. In contrast, the streamwise velocity contours of the undulating whisker demonstrate a zigzag pattern, well-correlated with the peak and trough locations. Little or no reversed flow zone appears behind the peak, while a deep pack of reversed flow is seen behind the trough location. Overall, the wake recovery is faster in the case of the undulating whisker, which is further demonstrated by the comparison of wake structure in the horizontal planes, Fig. 6. The reduced reversed flow qualitatively agrees with that generated by whisker-shaped cylinder and a wavy cylinder in Miersch et al. (2011), Wang and Liu (2016), Zhang et al. (2005).

The contours of mean spanwise vorticity, ω_z, of the wake behind the undulating whisker exhibit pronounced periodicity along the whisker length. The well-organized positive and negative vorticity band are distributed alternately, revealing the counter-rotating vortices with respect to the peak or trough locations, Fig. 4. For the smooth whisker, the distribution of the spanwise vorticity is rather random, lack of periodicity.

The streamwise turbulence intensity (I_u) contours show a significant difference when comparing the smooth and undulating whiskers, Fig. 5. While the wake region of high turbulence intensity (15%) is

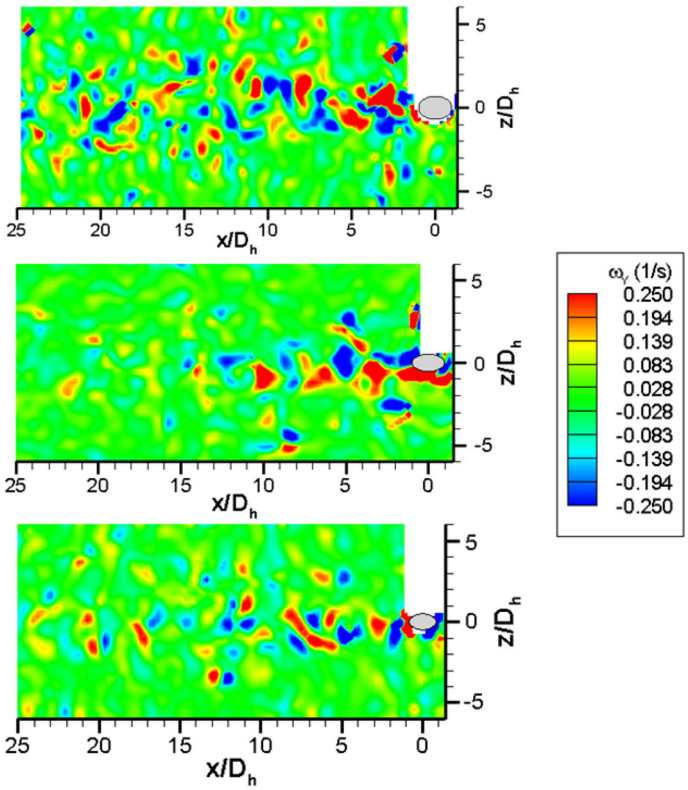

Fig. 10 Instantaneous vertical vorticity ω_y (1/s) in the horizontal plane at Re = 390 and AOA = 0°. The smooth California sea lion whisker (top), the peak location (middle), and the trough location (bottom) of an undulating elephant seal whisker. Flow is from right to left

extended as far as $30D_h$ away from the smooth whisker, the wake region behind the undulating whisker of a similar level of turbulence is remarkably reduced to just $10\,D_h$, one-third of the former case. From $20-70\,D_h$, the streamwise turbulence intensity is at the level of 4–5% for the undulating whisker, close to the inflow condition. In contrast, the wake does not recover to the mean flow turbulence level even at 70 D_h for the smooth whisker. The dramatic reduction in area of high turbulence can be seen in both peak and trough locations, which is a strong indicator of the suppressed vortex shedding mechanism, consistent with results in Wang and Liu (2016).

3.2 Flow statistics of the wake: horizontal planes

Details of the wake in the horizontal planes corresponding to the peak and trough locations of the undulating whisker are also examined at an AOA = 0°. The reversed flow region has a similar width where it is about $2D_h$ long at the peak and double at the trough location. The noticeable reduction of the wake region has been observed in Wang and Liu (2016) and Raman et al. (2013), which is correlated to an increase of the axis aspect ratio (a/b and k/l) for non-circular shapes. As expected, the streamwise velocity recovers to 80% of the inflow speed at $10D_h$ and 90% of the inflow speed at $15D_h$ for the peak location at $z = 0$. At the trough location, consistent with the longer reversed flow region, the wake recovery is also delayed. The streamwise velocity is gradually increased but lower than 90% of the inflow speed until $30D_h$ downstream (at $z = 0$). Behind the smooth whisker, the streamwise velocity remains at 70–80% of the inflow speed up to 27 D_h, shown in Fig. 6. This result further elaborates the faster wake recovery in the case of the undulating whisker, from the overall trend as observed in the vertical center plane (Fig. 3).

The separated shear layers are indicated by the vertical vorticity (ω_y) contours, in Fig. 7. Compared with the symmetric vorticity contours of slow-dissipated vorticity, the strong vorticity is closer to the whisker. The undulating whisker shows a longer region of high vorticity, extending for 10 D_h, but then quickly dissipates to minor levels by 20 D_h downstream. While dissipating quickly in the streamwise direction, the vorticity in the wake of the undulating whisker also spreads out in the z-direction, an indicator of enhanced

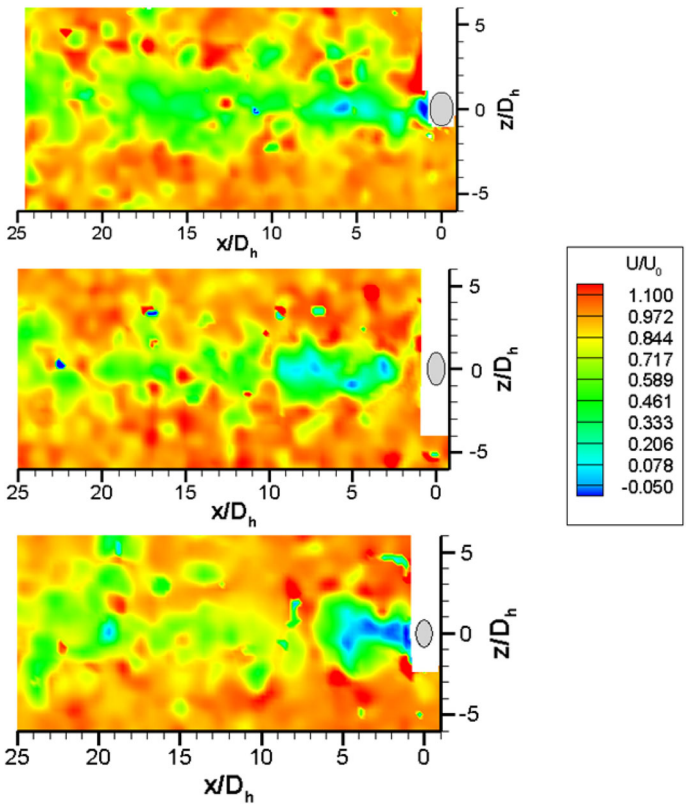

Fig. 11 Instantaneous streamwise velocity U/U_0 in the horizontal plane at Re = 390 and AOA = 90°. The smooth California sea lion whisker (top), the peak location (middle), and the trough location (bottom) of an undulating elephant seal whisker. Flow is from right to left

mixing in the wake. A clear difference is also seen in the peak and trough locations for the undulating whisker's wake.

The wake of the smooth whisker shows high levels of turbulence intensity, lasting for 15 D_h, Fig. 8. The maximum turbulence intensity remains at 9–10% at 27 D_h. The streamwise turbulence intensity in the peak and trough horizontal planes is dramatically lower than that in the wake of the smooth whisker. It is also very interesting to note a gap appears to form between the whisker and the area of the maximum turbulence intensity, which does not exist in the wake of the smooth whisker. This gap may explain why the undulating whisker is subjected to less influence from the vortex shedding.

3.3 Vortex shedding

Vortex shedding behavior is directly associated to the VIV of a bluff body in a flow path. Instantaneous velocities acquired at 5000 Hz in the horizontal planes are sufficient in temporal resolution to quantify the strength of vortex shedding. In particular, two cases of the AOA, 0° and 90°, are inspected for the effects of whisker orientation with respect to the incoming flow. The instantaneous streamwise velocities and vorticities at an AOA of 0°, Figs. 9 and 10, show a consistent trend with the previous ensemble-averaged results, Figs. 6 and 7. The wake region is significantly reduced at the peak location of the undulating whisker, compared to that of the smooth whisker. Furthermore, vertical vorticity remains at high magnitude up to 10 D_h at the peak and about 15 D_h at the trough location, versus 25 D_h downstream of the smooth whisker. The flow pattern observed from the high-speed PIV data confirms the wake suppression by the undulating whisker at AOA = 0°.

Significant changes in the streamwise velocity and vorticity appear once the orientation of whiskers is adjusted to an AOA = 90° (Figs. 11, 12). The wake region becomes wider and the velocity deficit is increased behind both the smooth and undulating whiskers, compared to the case of the AOA = 0°. The difference between the peak and trough location behind the undulating whisker is marginal; none of the

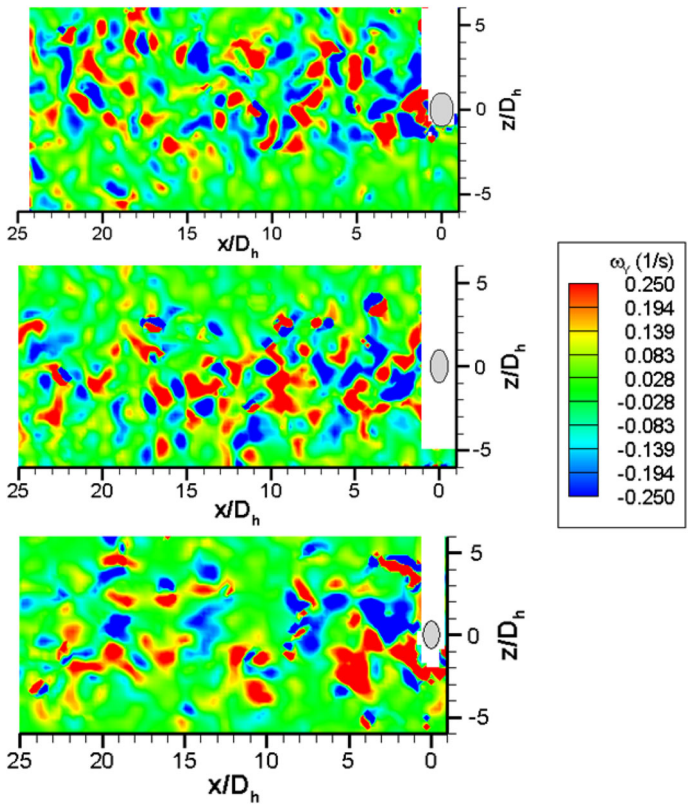

Fig. 12 Instantaneous vertical vorticity ω_y (1/s) in the horizontal plane at Re = 390 and AOA = 90°. The smooth California sea lion whisker (top), the peak location (middle), and the trough location (bottom) of an undulating elephant seal whisker. Flow is from right to left

locations show dissipation of vorticity by 25 D_h. The highly 3D vortex structures induced by an undulating whisker have been extensively illustrated in Witte et al. (2012) and Wang and Liu (2016). The wavy flow separation line on the whisker surface, counter-rotating vortices shed simultaneously from the double sides of the whisker are believed to contribute to the reduction of the drag and fluctuations. Limited by the spatial resolution, no detailed structure of periodic vortex shedding will be focused on. Instead, the frequency and magnitude of vortex shedding will be illustrated further.

Spectral analysis was performed to examine the distribution of turbulent kinetic energy across a range of frequencies in the wake of the smooth and undulating whiskers, Fig. 13. The spectra were calculated by taking the fast Fourier transform (FFT) of the instantaneous streamwise velocity at several locations of the separated shear layers. Localized high-energy signatures can be seen clearly at frequencies corresponding to periodic vortex shedding. A concentration of turbulent energy is indicated by the primary peak at the frequency of 108 Hz behind the smooth whisker, 150 and 158 Hz at the peak and trough of the undulating whisker at an AOA = 0°. Miersch et al. (2011) reported the frequency of seal and sea lion whiskers fall in the range of 47–193 Hz for a free-stream flow speed between 0.17 and 0.52 m/s. Our results appears to be aligned with this work. In addition, the power spectral density is found to be 50% lower for the case of the undulating whisker, indicating reduced strength of vortex shedding. This result is consistent with suppressed wake generated by the undulating whisker, as well as recent work of Morrison et al. (2016), Kim and Yoon (2017).

Once the AOA is changed to be 90°, the primary peak frequency shifts to a lower value for all three positions. This agrees with the trend of vortex shedding frequency reported by Kim and Yoon (2017) It is even more interesting to note a dramatic jump in the power spectral density for both smooth and undulating whiskers at AOA = 90°. The power spectral density is increased to 9 times higher for the smooth whisker. The increment of the power spectral density of the wake of undulating whisker is even more noticeable: 12 times higher in the peak location and 19 times higher in the trough location. This result indicates the vortex

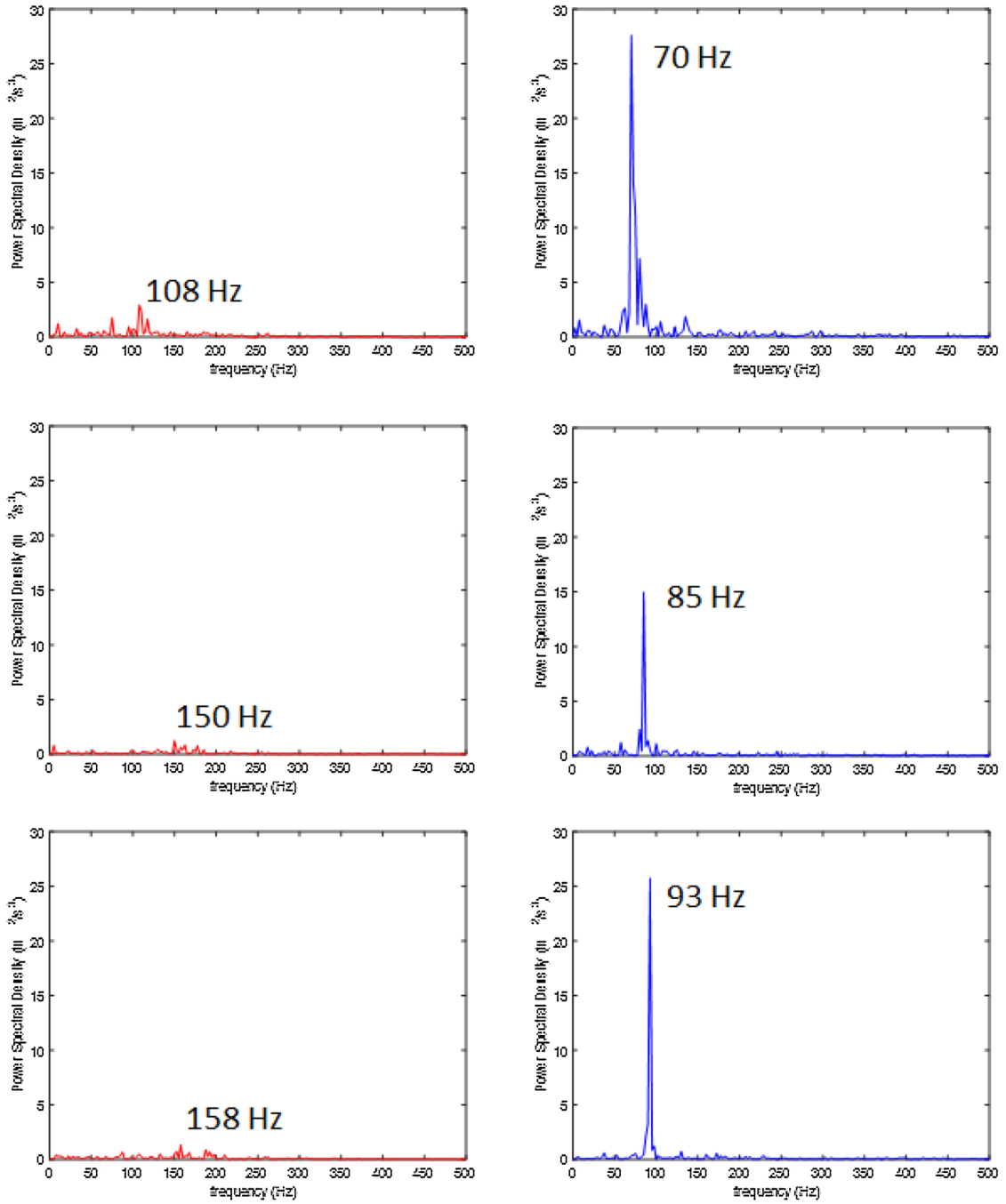

Fig. 13 Power spectrum of the velocities at selected locations of the wake at Re = 390. The smooth whisker of a California sea lion (top), the elephant seal whisker at the peak location (middle), and the elephant seal whisker at the trough location (bottom). AOA = 0° (left) and AOA = 90° (right)

shedding behavior is greatly affected by the AOA, which agreed to that in Murphy (2013). Our data also shows evidence of a lower power density in the wake of the undulating whisker, regardless the angle of attack, which is aligned with Kim and Yoon (2017) but distinctly different from Murphy (2013). In short, when the whisker's orientation is well aligned with respect to the incoming flow, VIV can be remarkably reduced. However, when the major axis presents a large AOA to the inflow, VIV can be substantially magnified, as reported in Beem and Triantafyllou (2015), Hans et al. (2014).

4 Conclusions and outlook

Experiments of the wake flow of a real undulating elephant seal whisker and a smooth sea lion whisker are conducted under well-controlled laboratory water channels. The turbulent statistics are achieved by a snapshot PIV and the vortex shedding behavior is quantified by a high-speed PIV method.

The ensemble-averaged flow properties show a reduced reversed flow region with quickly dissipated vorticity and significantly reduced turbulence levels in the wake of the undulating whisker. In spite of the naturally presented variation in whisker diameter and curvature, the distinct flow feature of wake suppression by the undulating whisker at an AOA of 0° is clear from observation of two orthogonal views. In particular, promoted mixing in the wake induced by the undulations may push the area of high-magnitude turbulence intensities away from the whisker itself, thus reduce the VIV.

Spectral analysis of high-speed PIV data indicates the reduced power spectra density behind the undulating whisker, compared to that of the smooth whisker, regardless of the AOA. However, changing the AOA from 0° to 90° substantially increases the power spectral density, thus augmenting the vortex shedding significantly.

Ongoing work is to directly measure the smooth and undulating whisker vibration from the high-speed PIV images and to examine the relation of the dominant whisker vibration frequency to the frequency of the vortex shedding in the wake. New experimental data will be obtained at a higher Reynolds number of 2000, based on the seal swimming speed and the whisker hydrodynamic diameter. This will help to further understand the effect the Reynolds number has on the wake flow and the vortex shedding behavior, as well as provide further insights into whisker-inspired engineering applications.

Acknowledgements This research is supported by the Faculty Startup Funds from the Office of Research at the Cleveland State University. The Authors would like to acknowledge Mr. David Epperly for assistance in experimental setup and the Civil Engineering Department for the access to the water channel. The authors also thank the NSF East Asia and Pacific Summer Institute for U.S. Graduate Students Program (NSF EAPSI 1515471) for the great opportunity to conduct high-speed PIV experiments at the Biofluid and Biomimic Research Center (BBRC) of the Pohang University of Science and Technology, Republic of Korea.

References

Adrian RJ, Westerweel J (2011) Particle image velocimetry. Cambridge University, New York

Beem H (2015) Passive wake detection using seal whisker-inspired sensing. PhD Dissertation, Joint Program in Oceanography and Applied Ocean Sciences and Engineering, MIT and WHOI, Cambridge

Beem H, Triantafyllou M (2015) Wake-induced slaloming response explains exquisite sensitivity of seal whisker-like sensor. J Fluid Mech 783:306–322

Boeuf B, Naito Y, Asaga T, Crocker D, Costa D (1992) Swim speed in a female northern elephant seal–metabolic and foraging implications. Can J Zool 70:786–795

Dehnhardt G, Kaminski A (1995) Sensitivity of the mystacial vibrissae of the harbour seals (*Phoca vitulina*) for size differences of actively touched objects. J Exp Biol 198(11):2317–2323

Fish F, Howle L, Murray M (2008) Hydrodynamic flow control in marine mammals. Integr Comp Biol 48(6):788–800. https://doi.org/10.1093/icb/icn029

Ginter C, DeWitt T, Fish F, Marshall C (2012) Fused traditional and geometric morphometerics demonstrate pinniped Whisker diversity. PLoS One 7(4):e34481

Ginter C, Fish F, Marshall C (2010) Morphological analysis of the bumpy profile of phocid vibrissae. Mar Mammal Sci 26:733–743

Hanke W, Witte M, Miersch LI, Grede M, Oeffner J, Michael M, Hanke F, Leader A, Denhardt G (2010) Harbor seal vibrissae morphology suppresses vortex-induced vibrations. J Exp Biol 213:2665–2672

Hans H, Miao J, Triantafyllou M (2014) Mechanical characteristics of harbor seal (Phoca vitulina) vibrissae under different circumstances and their implications on its sensing methodology. Bioinspiration Biomim 9:036013

Hans H, Miao J, Triantafyllou M, Weymouth G (2013) Whisker-like geometries and their force reduction properties, OCEANS MTS/IEEE Conference

James H, Dykes RW (1978) Some experiments on navigation in the harbour seal, Phoca vitulina. Anim Migr Navig Homing 7:395–404

Keane RD, Adrian RJ (1993) Theory and simulation of particle image velocimetry. In: Proceedings Volume 2052, fifth international conference on laser anemometry: advances and applications. https://doi.org/10.1117/12.150541

Kim HJ, Yoon HS (2017) Effect of the orientation of the harbor seal vibrissa based biomimetic cylinder on hydrodynamic forces and vortex induced frequency. AIP Adv 7:105015

Lin YF, Bai HL, Mahbub Alam Md, Zhang WG, Lam K (2016) Effects of large spanwise wavelength on the wake of sinusoidal wavy cylinder. J Fluids Struct 61:392–409

Miersch L, Hanke W, Wieskotten S, Hanke FD, Oeffner J, Leder A, Brede M, Witte M, Dehnhardt G (2011) Flow sensing by pinniped whiskers. Philos Trans R Soc B Biol Sci 366(1581):30773084

Morrison HE, Brede M, Dehnhardt G, Leder A (2016) Simulating the flow and trail following capabilities of harbour seal vibrissae with the lattice Boltzmann method. J Comput Sci 17:394402
Murphy C (2013) Structure and function of pinniped vibrissae, PhD Dissertation, University of South Florida
Murphy C, Reichmuth C, Eberhardt WC, Calhoun BH, Mann DA (2017) Seal whiskers vibrate over broad frequencies during hydrodynamic tracking. Sci Rep 7:8350
New T, Shi S, Liu Y (2015) On the flow behaviour of confined finite-length wavycylinders. J Fluids Struct 54:281296
Raffel M, Willert C, Werely S, Kompenhans J (2007) Particle image velocimetry: a practical guide. Springer, Berlin
Raman SK, Prakash KA, Vengadesan S (2013) Effect of axis ratio on fluid flow around an elliptic cylinder: a numerical study. J Fluids Eng 135:111201
Renouf D, Gaborko L (1982) Speed Sensing in harbour seal. J Mar Biol Assoc UK 62(01):227–228
Rinehart A, Shyam V, Zhang W (2017) Characterization of seal whisker morphology: implications for whisker-inspired flow control applications. Bioinspir Biomim 12:066005
Shyam V, Ameri A, Pointsatte P, Thurman D, Wroblewski A, Synder C 2015) Application of pinniped vibrissae to aeropropulsion. In: Proceedings of ASME Turbo Expo
Tavoularis S (2005) Measurements in fluid mechanics. Cambridge University Press, Cambridge, p 48
Wang S, Liu Y (2016) Wake dynamics behind seal-vibrissa-shaped cylinder: a comparative study by time-resolved particle velocimetry measurements. Exp Fluids 57:32. https://doi.org/10.1007/s00348-016-2117-9
Wieneke B (2015) PIV uncertainty quantification from correlation statistics. Meas Sci Technol 26(7):110
Witte M, Hanke W, Wieskotten S, Miersch L, Brede M, Dehnhardt G, Leder A (2012) PIV measurements of the near-wake behind a sinusoidal cylinder. Nat Inspir Fluid Mech NNFM 119:271289
Zhang W, Daichin Lee SJ (2005) PIV measurements of the near-wake behind a sinusoidal cylinder. Exp Fluids 38:824–832